Multicenter analysis of high-resolution computed tomography and positron emission tomography/computed tomography findings to choose therapeutic strategies for clinical stage IA lung adenocarcinoma

Morihito Okada, MD, PhD,[a] Haruhiko Nakayama, MD, PhD,[b] Sakae Okumura, MD, PhD,[c] Hiromitsu Daisaki, PhD,[d] Shuji Adachi, MD, PhD,[e] Masahiro Yoshimura, MD, PhD,[f] and Yoshihiro Miyata, MD, PhD[a]

Objective: The detection rates of small lung cancers, especially adenocarcinoma, have recently increased. An understanding of malignant aggressiveness is critical for the selection of suitable therapeutic strategies, such as sublobar resection. The objective of this study was to examine the malignant biological behavior of clinical stage IA adenocarcinoma and to select therapeutic strategies using high-resolution computed tomography, fluorodeoxyglucose-positron emission tomography/computed tomography, and a pathologic analysis in the setting of a multicenter study.

Methods: We performed high-resolution computed tomography and fluorodeoxyglucose-positron emission tomography/computed tomography in 502 patients with clinical T1N0M0 adenocarcinoma before they underwent surgery with curative intent. We evaluated the relationships between clinicopathologic characteristics and maximum standardized uptake values on fluorodeoxyglucose-positron emission tomography/computed tomography, ground-glass opacity ratio, and tumor disappearance rate on high-resolution computed tomography and component of bronchioloalveolar carcinoma on surgical specimens, as well as between these and surgical findings. We used a phantom study to correct the serious limitation of any multi-institution study using positron emission tomography/computed tomography, namely, a discrepancy in maximum standardized uptake values among institutions.

Results: Analyses of receiver operating characteristic curves identified an optimal cutoff value to predict high-grade malignancy of 2.5 for revised maximum standardized uptake values, 20% for ground-glass opacity ratio, 30% for tumor disappearance rate, and 30% for bronchioloalveolar carcinoma ratio. Maximum standardized uptake values and bronchioloalveolar carcinoma ratio, tumor disappearance rate, and ground-glass opacity ratio mirrored the pathologic aggressiveness of tumor malignancy, nodal metastasis, recurrence, and prognosis, including disease-free and overall survival.

Conclusions: Maximum standardized uptake value is a significant preoperative predictor for surgical outcomes. High-resolution computed tomography and fluorodeoxyglucose-positron emission tomography/computed tomography findings are important to determine the appropriateness of sublobar resection for treating clinical stage IA adenocarcinoma of the lung. (J Thorac Cardiovasc Surg 2011;141:1384-91)

From the Department of Surgical Oncology,[a] Hiroshima University, Hiroshima, Japan; Department of Thoracic Surgery,[b] Kanagawa Cancer Center, Yokohama, Japan; Department of Thoracic Surgery,[c] Cancer Institute Hospital, Tokyo, Japan; Department of Radiology,[d] National Cancer Center, Tokyo, Japan; and Department of Radiology[e] and Thoracic Surgery,[f] Hyogo Cancer Center, Akashi, Japan.

Disclosures: Authors have nothing to disclose with regard to commercial support.

Received for publication Nov 26, 2010; revisions received Jan 21, 2011; accepted for publication Feb 9, 2011; available ahead of print March 28, 2011.

Address for reprints: Morihito Okada, MD, PhD, Department of Surgical Oncology, Research Institute for Radiation Biology and Medicine, Hiroshima University, 1-2-3-Kasumi, Minami-ku, Hiroshima City, Hiroshima 734-0037, Japan (E-mail: morihito@hiroshima-u.ac.jp).

0022-5223/$36.00

doi:10.1016/j.jtcvs.2011.02.007

The standard treatment for operable non–small cell lung cancer, even early clinical T1N0M0 disease, remains lobectomy with dissection of the hilar and mediastinal lymph nodes.[1] However, clinical investigations to date have demonstrated that sublobar resection, which chiefly consists of radical segmentectomy with nodal dissection, might be feasible for treating early lung cancers with the tangible advantages of maintained lung function and a reasonable prognosis.[2,3] To date, there are no means to preoperatively identify early lung cancers that are biologically less aggressive and may be better suited for a sublobar resection.

Recent advances in high-resolution computed tomography (HRCT) and the widespread application of computed tomography (CT) screening have enhanced the discovery of small lung cancers, particularly adenocarcinoma.[2,3] These early-stage cancers are biologically heterogeneous, and the malignant aggressiveness is not well characterized

Abbreviations and Acronyms

AUC	= area under the curve
BAC	= bronchioloalveolar carcinoma
CT	= computed tomography
DFS	= disease-free survival
FDG	= F-18 fluorodeoxyglucose
FOV	= field of view
GGO	= ground-glass opacity
HRCT	= high-resolution computed tomography
maxSUV	= maximum standardized uptake value
PET	= positron emission tomography
ROC	= receiver operating characteristic
SUV	= standardized uptake value
TDR	= tumor disappearance rate

at the time of diagnosis. This information should be considered in selecting the therapeutic strategy.

Positron emission tomography (PET)/CT with F-18 fluorodeoxyglucose (FDG) has become an integral part of the non–small cell lung cancer evaluation.[4-6] This modality generates quantitative images based on glucose metabolism reflecting the metabolic activity and proliferative potential of malignant tumors, and providing anatomic CT images. Small-scale studies have demonstrated the role of FDG-PET/CT in assessing the biological status of cancers,[7,8] but this requires confirmation in a larger cohort. Therefore, assessed the biological nature of small adenocarcinomas in more than 500 patients by using HRCT and FDG-PET/CT and the pathologic findings of surgical specimens in a multicenter setting. Because of the heterogeneity of PET techniques and performance, we corrected inter-institutional errors in maximum standardized uptake values (maxSUVs) resulting from PET/CT scanners of variable quality based on outcomes of a study using an anthropomorphic body phantom that conformed to National Electrical Manufacturers Association standards.[9]

PATIENTS AND METHODS

We enrolled 502 patients (female, 279 [56%]; male, 223 [44%]; mean age, 65.3 ± 9.6 years) with clinical T1N0M0 stage IA adenocarcinoma of the lung at 4 institutions between August 1, 2005, and December 31, 2009. All patients underwent HRCT and FDG-PET/CT followed by curative R0 resection. The ethics committees at each institution approved this multicenter study and the prospective database used in the analysis.

High-Resolution Computed Tomography

Chest images were obtained using 16-row multidetector CT independently of subsequent PET/CT examinations. High-resolution images of the tumors were acquired using the following parameters: 120 kVp, 200 mA, 1- to 2-mm section thickness, 512 × 512 pixel resolution, 0.5- to 1-second scanning time, a high spatial reconstruction algorithm with a 20-cm field of view (FOV) and mediastinal (level, 40 HU; width, 400

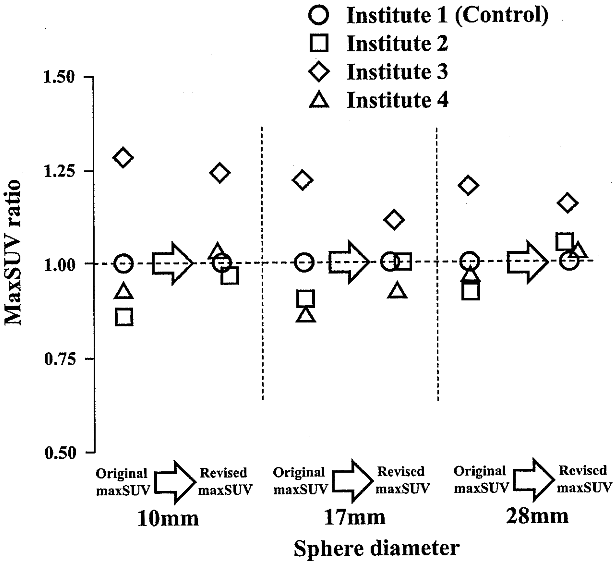

FIGURE 1. maxSUV adjusted using experimental phantom (revised maxSUV). Original maxSUV data were calibrated by multiplying calibration factors based on phantom studies to correct inter-institutional SUV variability. MaxSUV ratio is expressed as maxSUV of each institute for maxSUV of control institute (Institute 1). *maxSUV,* Maximum standardized uptake value.

HU) and lung (level, −600 HU; width, 1600 HU) window settings. Ground-glass opacity (GGO) was defined as a misty increase in lung attenuation without obscuring the underlying vascular markings, and we defined the GGO ratio (%) as [1− (maximum dimension of consolidation of lung windows/maximum dimension of tumor of lung windows)] × 100. Tumor disappearance rate (TDR) (%) was defined as [1−(tumor area of the mediastinal windows/tumor area of the lung windows)] × 100.[2,3,10]

Fluorodeoxyglucose-Positron Emission Tomography/ Computed Tomography

The patients fasted for more than 4 hours before being intravenously injected with 74-370 MBq of FDG, and then relaxed for at least 1 hour before FDG-PET/CT scanning. Blood glucose was calculated before tracer injection to confirm a level of less than 150 mg/dL.[11] Patients with blood glucose values of 150 mg/dL or greater were excluded from PET/CT acquisition. Images were obtained in this study using Discovery ST (GE Healthcare, Buckinghamshire, England), Aquiduo (Toshiba Medical Systems Corporation, Tochigi, Japan), or Biograph Sensation16 (Siemens Healthcare, South Iselin, NJ) integrated PET/CT scanners. Low-dose unenhanced CT images of a 2- to 4-mm section thickness for attenuation correction and localization of lesions identified by PET were obtained from the head to the pelvic floor of each patient using a standard protocol. Immediately after CT, PET covered the identical axial FOV for 2 to 4 minutes per table position depending on the condition of the patient and scanner performance. All PET images with a 50-cm FOV were reconstructed using an iterative algorithm with CT-derived attenuation correction. Variations in standardized uptake value (SUV) among institutions were minimized using the anthropomorphic body phantom. A calibration factor was analyzed by dividing the actual SUV by the gauged mean SUV in the phantom background to decrease inter-institutional SUV inconsistencies, and the final maxSUV used in this is referred to as revised maxSUV. The adjustment of the inter-institutional variability in SUV narrowed the range from 0.89 to 1.24 to 0.97 to 1.18 when maxSUV ratio was expressed as the maxSUV of each institute for the maxSUV of the control institute (Figure 1).

GTS

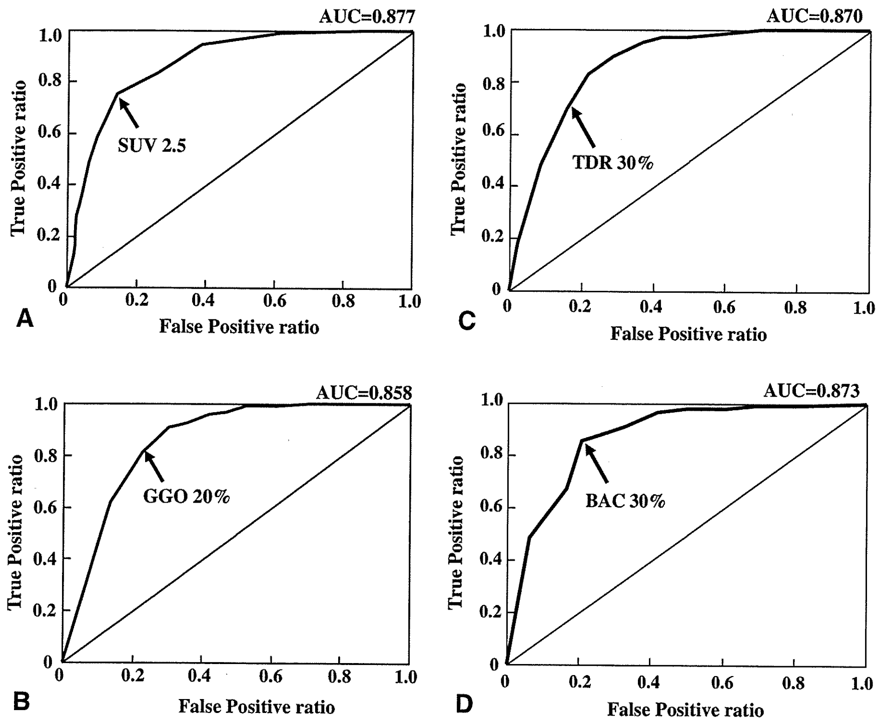

FIGURE 2. ROC curves for positive predictive values of pathologic lymph node metastasis, lymphatic invasion, blood vessel invasion, or pleural invasion. ROC curves are for revised maxSUV (A), GGO ratio (B), TDR (C), and BAC ratio (D). *maxSUV,* Maximum standardized uptake value; *GGO,* ground-glass opacity; *TDR,* tumor disappearance rate; *BAC,* bronchioloalveolar carcinoma; *AUC,* area under the curve; *SUV,* standardized uptake value.

Resected tumors were fixed in 10% formalin, embedded in paraffin, and pathologically evaluated (including the largest cut) using hematoxylin–eosin and Elastica van Gieson staining. The amount of bronchioloalveolar carcinoma (BAC) areas proportionate to whole tumors was approximately calculated as the BAC ratio. Independent observers and pathologists blindly evaluated GGO and BAC ratios and TDR, and corrected discrepancies among evaluations using mean values.

Receiver operating characteristic (ROC) curves of the revised maxSUV, GGO ratios, TDR, and BAC ratios to predict lymphatic, blood vessel, and pleural invasion or nodal involvement were generated to determine the cutoff values that yielded optimal sensitivity and specificity. The patient population was subdivided on the basis of the cutoff values of the revised SUVmax, GGO, TDR, and BAC ratios derived from ROC curves. We performed multiple logistic regression analyses to demonstrate independent variables of maxSUV, GGO ratio, TDR, and BAC ratio relative to the prediction of pathologic findings for high malignant grade and recurrence. Survival was calculated using the Kaplan–Meier method, and differences were determined using the log-rank test. Disease-free survival (DFS) was defined as time from date of surgery until the first event (relapse or death from any cause) or last follow-up. Overall survival was defined as time from the date of surgery until death from any cause or last follow-up.

RESULTS

The primary tumor measured by HRCT was 20 mm or less in diameter in 290 patients (58%) and 21 to 30 mm in 212 patients (42%). Lymphatic permeation, blood vessel, and pleural invasion was evident in 76 patients (15%), 92 patients (18%), and 56 patients (11%), respectively, and lymph nodes were involved in 38 (8%) of them.

The ROC curves identified optimal revised maxSUV, GGO, TDR, and BAC ratio cutoff values of 2.5 (area under the curve [AUC], 0.877), 20% (AUC, 0.858), 30% (AUC, 0.870), and 30% (AUC, 0.873), respectively, for predicting pathologic findings of high malignancy (Figure 2). At a cutoff value of 2.5, a high revised maxSUV significantly correlated with male gender, a high CEA value, large tumor, lymphatic invasion, vascular invasion, pleural invasion, and lymph node metastasis (Table 1). Likewise, low TDR, GGO, and BAC ratios were significantly associated with a high CEA value, lymphatic, vascular, pleural invasion, and lymph node metastasis. Possible predictors for lymphatic, vascular, and pleural invasion, and nodal metastasis and recurrence were investigated (Table 2). Revised maxSUV, GGO ratio, TDR, and BAC ratio were all significant determinants for predicting lymphatic permeation, vascular and pleural invasion, nodal metastasis, and recurrence. However, the odds ratios indicated that revised maxSUV and the BAC ratio revealed biological aggressive tumor grade more effectively than GGO ratio and TDR.

A significant difference in DFS was identified (Figure 3) between patients whose adenocarcinoma had revised maxSUV 2.5 or less ($n = 343$; 3-year DFS rate, 96%) and greater than 2.5 ($n = 159$; 3-year DFS rate, 77%; $P < .001$). We also found significant differences in DFS between patients whose adenocarcinoma had GGO ratios of

TABLE 1. Clinical characteristics of patients with cT1N0M0 adenocarcinoma (n = 502)

	Patients (n = 502)	Revised maxSUV ≤2.5/>2.5 (n = 343/159)	*P* value	GGO ratio ≥20%/<20% (n = 304/198)	*P* value	TDR ≥30%/<30% (n = 346/156)	*P* value	BAC ratio ≥30%/<30% (n = 304/198)	*P* value
Age (y) (means ±SD)	65.3 ± 9.6	65.3 ± 9.4/65.5 ±9.8	.8380	65.0 ± 9.3/65.9 ± 10.0	.2790	64.7 ± 9.4/66.7 ± 9.9	.0365	65.4 ± 9.5/65.3 ± 9.7	.9054
Gender									
Male	223	140/83	.0169	119/104	.0032	144/79	.0597	113/110	<.0001
Female	279	203/76		185/94		202/77		191/88	
CEA (ng/mL)									
≤5	449	321/128	<.0001	289/160	<.0001	324/125	<.0001	284/165	.0003
>5	53	22/31		15/38		22/31		20/33	
Tumor size (mm)									
T ≤20	290	218/72	.0001	183/107	.1723	213/77	.0104	180/110	.4178
<20 T ≤30	212	125/87		121/91		133/79		124/88	
Ly permeation									
positive	76	15/61	<.0001	13/63	<.0001	25/51	<.0001	12/64	<.0001
negative	426	328/98		291/135		321/105		292/134	
V invasion									
positive	92	16/76	<.0001	15/77	<.0001	23/69	<.0001	11/81	<.0001
negative	410	327/83		289/121		323/87		293/117	
P invasion									
positive	56	12/44	<.0001	10/46	<.0001	14/42	<.0001	6/50	<.0001
negative	446	331/115		294/152		332/114		298/148	
N metastasis									
positive	38	10/28	<.0001	8/30	<.0001	10/28	<.0001	5/33	<.0001
negative	464	333/131		296/168		336/128		299/165	

CEA, Carcinoembryonic antigen; *Ly,* lymphatic; *V,* blood vessel; *P,* pleural; *N,* lymph node; *maxSUV,* maximum standardized uptake value; *GGO,* ground-glass opacity; *TDR,* tumor disappearance rate; *BAC,* bronchioloalveolar carcinoma.

TABLE 2. Analysis of possible predictors for Ly factor, V factor, P factor, N factor, and recurrence status

Factors total (n = 502)	Favorable	Unfavorable	Odds ratio (95% CI)	*P* value
Positive Ly factor (n = 76)				
Revised maxSUV	≤2.5	>2.5	13.61 (7.41–25.01)	<.0001
GGO ratio	≥20%	<20%	10.45 (5.56–19.63)	<.0001
TDR	≥30%	<30%	6.24 (3.68–10.56)	<.0001
BAC ratio	≥30%	<30%	11.62 (6.07–22.25)	<.0001
Positive V factor (n = 92)				
Revised maxSUV	≤2.5	>2.5	18.71 (10.37–33.78)	<.0001
GGO ratio	≥20%	<20%	12.26 (6.78–22.17)	<.0001
TDR	≥30%	<30%	11.14 (6.57–18.88)	<.0001
BAC ratio	≥30%	<30%	18.44 (9.48–35.87)	<.0001
Positive P factor (n = 56)				
Revised maxSUV	≤2.5	>2.5	10.55 (5.39–20.68)	<.0001
GGO ratio	≥20%	<20%	8.90 (4.37–18.12)	<.0001
TDR	≥30%	<30%	8.74 (4.60–16.59)	<.0001
BAC ratio	≥30%	<30%	16.78 (7.03–40.03)	<.0001
Positive N factor (n = 38)				
Revised maxSUV	≤2.5	>2.5	7.12 (3.36–15.07)	<.0001
GGO ratio	≥20%	<20%	6.61 (2.96–14.74)	<.0001
TDR	≥30%	<30%	7.35 (3.47–15.56)	<.0001
BAC ratio	≥30%	<30%	11.96 (4.58–31.22)	<.0001
Positive recurrence (n = 29)				
Revised maxSUV	≤2.5	>2.5	7.71 (3.22–18.46)	<.0001
GGO ratio	≥20%	<20%	8.25 (3.09–22.01)	<.0001
TDR	≥30%	<30%	4.66 (2.11–10.28)	<.0001
BAC ratio	≥30%	<30%	10.84 (3.71–31.66)	<.0001

Ly, Lymphatic permeation; *V,* blood vessel invasion; *P,* pleural invasion; *N,* lymph node metastasis; *maxSUV,* maximum standardized uptake value; *GGO,* ground-glass opacity; *TDR,* tumor disappearance rate; *BAC,* bronchioloalveolar carcinoma.

GTS

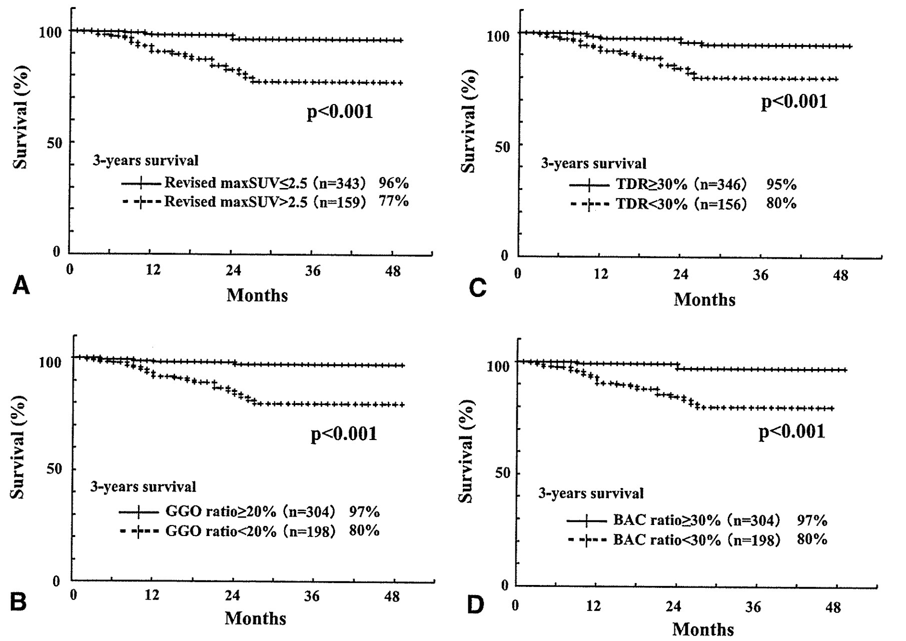

FIGURE 3. DFS curves according to grade of revised maxSUV (A), GGO ratio (B), TDR (C), and BAC ratio (D). *maxSUV,* Maximum standardized uptake value; *GGO,* ground-glass opacity; *TDR,* tumor disappearance rate; *BAC,* bronchioloalveolar carcinoma.

20% or more (n = 304; 3-year DFS rate, 97%) and less than 20% (n = 198; 3-year DFS rate, 80%; $P < .001$), between those whose adenocarcinoma had TDR 30% or more (n = 346; 3-year DFS rate, 95%) and less than 30% (n = 156; 3-year DFS rate, 80%; $P < .001$) and between those whose adenocarcinoma had BAC ratios of 30% or more (n = 304; 3-year DFS rate, 97%) and less than 30% (n = 198; 3-year DFS rate, 80%; $P < .001$). Revised maxSUV ($P = .016$) and GGO ($P = .024$) and pathologic BAC ($P = .005$) ratios were significant prognostic factors

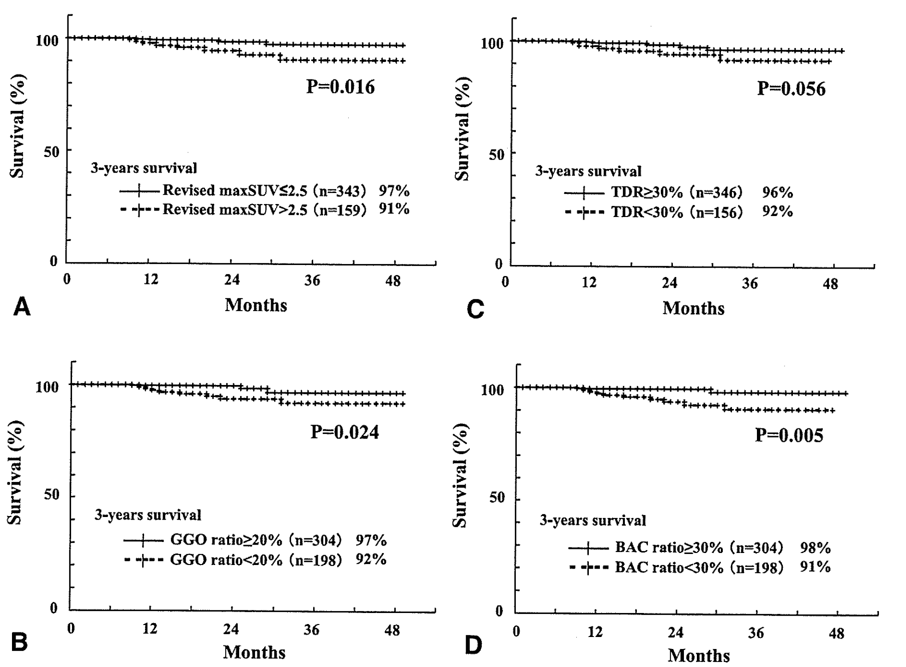

FIGURE 4. Overall survival curves according to grade of revised maxSUV (A), GGO ratio (B), TDR (C), and BAC ratio (D). *maxSUV,* Maximum standardized uptake value; *GGO,* ground-glass opacity; *TDR,* tumor disappearance rate; *BAC,* bronchioloalveolar carcinoma.

TABLE 3. Relationship between ground-glass opacity/tumor disappearance rate and revised maxSUV as predictors for Ly factor, V factor, P factor, N factor, and recurrence status

	Revised maxSUV	Ly permeation (+)/(-)	V invasion (+)/(-)	P invasion (+)/(-)	N metastasis (+)/(-)	Recurrence (+)/(-)
GGO ≤50% and TDR ≤50%	≤1.5	2/46	1/47	3/45	0/48	0/48
(n = 259)	(n = 48)	(4%)	(2%)	(6%)	(0)	(0)
	<1.5 ≤2.5	10/58	14/54	8/60	8/60	3/65
	(n = 68)	(15%)	(21%)	(12%)	(12%)	(4%)
	2.5<	59/84	73/70	43/100	27/116	22/121
	(n = 143)	(41%)	(51%)	(30%)	(19%)	(15%)
>50% GGO or >50% TDR	≤1.5	2/178	1/179	0/180	1/179	2/178
(n = 243)	(n = 180)	(1%)	(1%)	(0)	(1%)	(1%)
	<1.5 ≤2.5	1/46	0/47	1/46	1/46	2/45
	(n = 47)	(2%)	(0)	(2%)	(2%)	(4%)
	2.5<	2/14	3/13	1/15	1/15	0/16
	(n = 16)	(13%)	(19%)	(6%)	(6%)	(0)

maxSUV, Maximum standardized uptake value; *Ly,* lymphatic; *V,* blood vessel; *P,* pleural; *N,* lymph node; *GGO,* ground-glass opacity; *TDR,* tumor disappearance rate.

for overall survival, whereas TDR ($P = .056$) was marginally significant (Figure 4).

We examined the relationships between HRCT findings and maxSUV for predicting tumor invasiveness, nodal metastasis, and recurrence (Table 3). Generally, solid tumors on HRCT with GGO 50% or less and TDR 50% or less had high maxSUV and were more frequently associated with high malignant grade, nodal metastasis, and recurrence. However, solid tumors with lower maxSUV were associated with low malignant grade and far less nodal metastasis and recurrence. Among patients with tumors showing GGO 50% or less and TDR 50% or less, 19% and 15% of those with a revised maxSUV greater than 2.5 had nodal metastasis and recurrence, respectively,

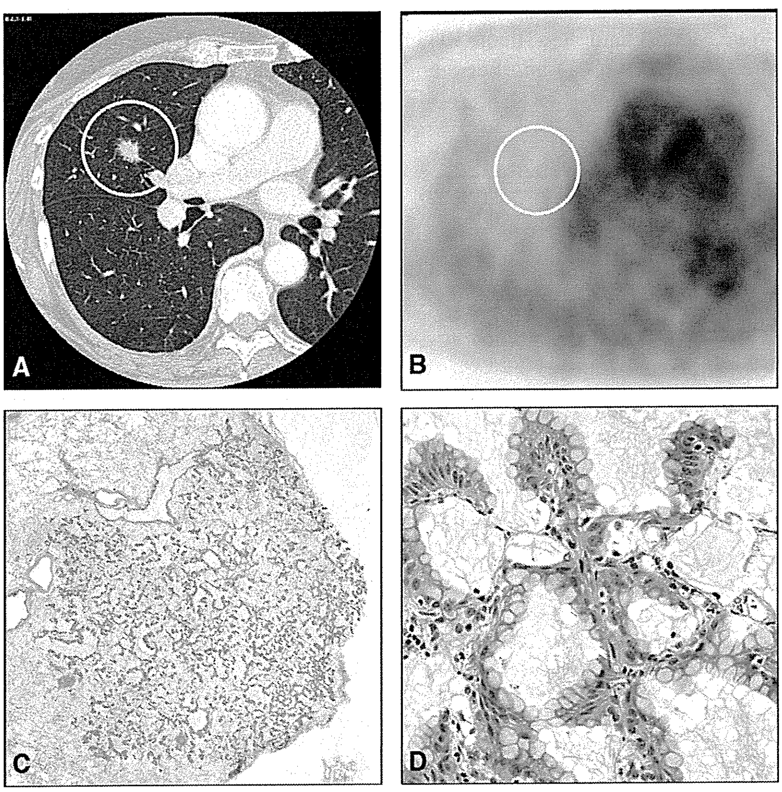

FIGURE 5. Tumor (1.5 cm in diameter) located at right middle lobe. A, HRCT findings show GGO ratio of 5%. B, PET/CT findings show no accumulation. Microscope findings show BAC with mucin formation (C and D, staining with hematoxylin–eosin at ×25 and ×200 magnification, respectively).

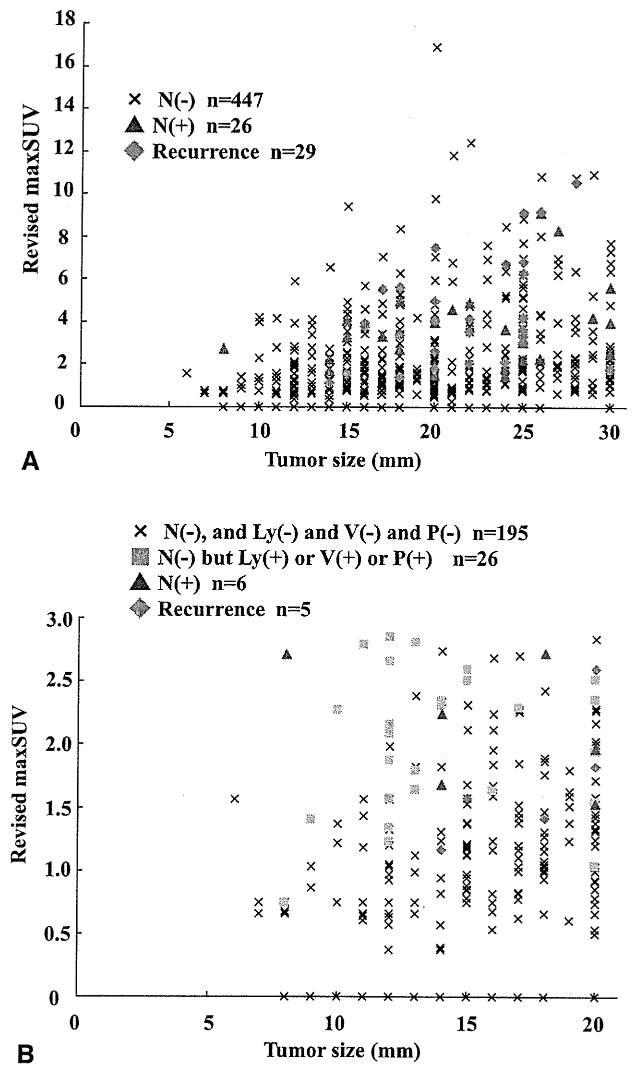

FIGURE 6. Relationship between tumor size and revised maxSUV level in cT1N0M0 adenocarcinomas. A, All patients. B, Tumor size ≤ 20 mm and revised maxSUV ≤ 3.0. Nodal metastasis (*triangles*); recurrence (*rhombi*); lymphatic, vascular, or pleural invasion without nodal metastasis (*squares*). *maxSUV,* Maximum standardized uptake value; *N,* lymph node; *Ly,* lymphatic; *V,* blood vessel; *P,* pleural.

whereas those with tumors showing revised maxSUV 1.5 or less had neither nodal metastasis nor recurrence.

DISCUSSION

The frequency of identifying small lung cancers has recently increased since CT and enhanced scanning have become routine procedures and surgeons have thus been able to assess the advantages of sublobar resection, such as radical segmentectomy instead of lobectomy.[2,3] The biological malignancy of small adenocarcinoma has generally been evaluated on the basis of HRCT findings. The specificity, sensitivity, and accuracy of radiologic diagnoses with HRCT on lymphatic/vessel invasion and nodal involvement of clinical T1N0M0 adenocarcinoma have been examined in a large prospective study (JCOG0201).[12] The conclusions failed to corroborate predetermined criteria using GGO ratio and TDR for specificity, and thus applicants for radical sublobar resection could not be suitably confirmed on the basis of criteria generated from HRCT findings. Therefore, the development of a novel tool that surpasses the diagnostic ability of HRCT is a current challenge.

Phase III randomized trials of standard lobectomy versus experimental limited resection for small (≤2 cm in diameter) peripheral non–small cell lung cancers are ongoing in the United States (CALGB-140503) and in Japan (JCOG0802/WJOG4607L). Because the biological behavior of several types of small lung cancers is aggressive, to detect indolent lung cancers preoperatively with radiographic imaging is important for the standardization of sublobar resection, although accurate radiographic definition of tumor extension and metastasis is challenging. We previously demonstrated that maxSUV on FDG-PET/CT is a potentially promising parameter of the degree of malignancy among cT1N0M0 lung adenocarcinoma.[7,8] However, relatively few patients were analyzed and postoperative survival data were obtained during a short period. We therefore performed an extended, larger multicenter study. To our knowledge, a large scale multi-institutional study of malignant tumor grade analyzed using PET/CT has not been reported.

The present analyses revealed that adenocarcinoma with high maxSUV and low GGO ratio, TDR, or BAC ratio is more closely associated with lymphatic, vessel, pleural invasion, lymph node metastasis, and recurrence. We also found a closer association between serum CEA levels and maxSUV, GGO ratio, TDR, and BAC ratio, which is preoperatively vital in uncovering patients at high risk of potential advanced disease.[13,14] High maxSUV was also a poor prognostic determinant for DFS and overall survival. These outcomes suggested that maxSUV can be a realistic surrogate marker of tumor malignancy grade and that FDG-PET/CT in addition to HRCT is a potent prognostic modality with which to detect patients at high risk of recurrence after curative resection of small adenocarcinoma.

Because PET/CT imaging reflects metabolic activity as glucose metabolism whereas HRCT generates only anatomic images, findings of PET/CT could be more powerful clinical predictors of biological tumor performance than those of HRCT. Most solid tumors on HRCT have high maxSUV and aggressive malignant behavior, whereas solid tumors with lower maxSUV were less aggressive. Figure 5 shows a mucinous BAC with indolent behavior that appeared as a solid tumor on HRCT with no accumulation on PET/CT.

We analyzed the association between tumor size and maxSUV in cT1N0M0 adenocarcinoma (Figure 6). A larger tumor was associated with a higher maximum SUV, and both size and maxSUV can predict tumor invasiveness, nodal metastasis, and recurrence. The figures show a notable tendency of small adenocarcinoma with high maxSUV to have more malignant features than larger adenocarcinoma with low maxSUV.

One of the major limitations of multicenter trials using PET is the wide variation in SUV among institutions. Many factors, such as preparation procedures, scan acquisition, image reconstruction, and data analysis affect SUV,[15,16] although semiquantitative SUV in patients with cancer is extensively applied to diagnose, stage, and evaluate therapeutic effectiveness.[4-6] Westerterp and colleagues[17] reported that a discrepancy in SUV of up to 30% among institutions could create a significant problem for multicenter studies. Inter-institutional variability in SUV obtained in the present study was minimized using an anthropomorphic body phantom. Therefore, quantitative SUVs adjusted by phantom studies can be dependable, and such correction will help to overcome one major limitation of multicenter of PET studies.

CONCLUSIONS

The findings of HRCT and FDG-PET/CT are important to select therapeutic strategies for treating c-stage IA adenocarcinoma of the lung, and maxSUV on FDG-PET/CT is an especially significant preoperative predictor for surgical outcomes. Sublobar resection might be performed in patients with adenocarcinoma with maxSUV 1.5 or less, and lymphadenectomy is required for tumors with maxSUV greater than 1.5.

References

1. Ginsberg RJ, Rubinstein LV. Randomized trial of lobectomy versus limited resection for T1N0 non-small cell lung cancer. Lung Cancer Study Group. *Ann Thorac Surg*. 1995;60:615-22.
2. Okada M, Koike T, Higashiyama M, Yamato Y, Kodama K, Tsubota N. Radical sublobar resection for small-sized non-small cell lung cancer: a multicenter study. *J Thorac Cardiovasc Surg*. 2006;132:769-75.
3. Nakayama H, Yamada K, Saito H, Oshita F, Ito H, Kameda Y, et al. Sublobar resection for patients with peripheral small adenocarcinomas of the lung: surgical outcome is associated with features on computed tomographic imaging. *Ann Thorac Surg*. 2007;84:1675-9.
4. Pieterman RM, van Putten JW, Meuzelaar JJ, Mooyaart EL, Vaalburg W, Koëter GH, et al. Preoperative staging of non-small-cell lung cancer with positron-emission tomography. *N Engl J Med*. 2000;343:254-61.
5. Vansteenkiste J, Fischer BM, Dooms C, Mortensen J. Positron-emission tomography in prognostic and therapeutic assessment of lung cancer: systematic review. *Lancet Oncol*. 2004;5:531-40.
6. Juweid ME, Cheson BD. Positron-emission tomography and assessment of cancer therapy. *N Engl J Med*. 2006;354:496-507.
7. Okada M, Tauchi S, Iwanaga K, Mimura T, Kitamura Y, Watanabe H, et al. Associations among bronchioloalveolar carcinoma components, positron emission tomographic and computed tomographic findings, and malignant behavior in small lung adenocarcinomas. *J Thorac Cardiovasc Surg*. 2007;133:1448-54.
8. Nakayama H, Okumura S, Daisaki H, Kato Y, Uehara H, Adachi S, et al. Value of integrated positron emission tomography revised using a phantom study to evaluate malignancy grade of lung adenocarcinoma: a multicenter study. *Cancer*. 2010;116:3170-7.
9. Mawlawi O, Podoloff DA, Kohlmyer S, Williams JJ, Stearns CW, Culp RF, et al. Performance characteristics of a newly developed PET/CT scanner using NEMA standards in 2D and 3D modes. *J Nucl Med*. 2004;45:1734-42.
10. Shimizu K, Yamada K, Saito H, Noda K, Nakayama H, Kameda Y, et al. Surgically curable peripheral lung carcinoma. Correlation of thin-section CT findings with histologic prognostic factors and survival. *Chest*. 2005;127:871-8.
11. Delbeke D, Coleman RE, Guiberteau MJ, Brown ML, Royal HD, Siegel BA, et al. Procedure guideline for tumor imaging with 18F-FDG PET/CT 1.0. *J Nucl Med*. 2006;47:885-95.
12. Suzuki K, Koike T, Shibata T, Kusumoto M, Asamura H, Nagai K, et al. Evaluation of radiologic diagnosis in peripheral clinical IA lung cancers. A prospective study for radiological diagnosis of peripheral early lung cancer (JCOG0201). *J Clin Oncol*. 2006;24:7220.
13. Okada M, Nishio W, Sakamoto T, Uchino K, Yuki T, Nakagawa A, et al. Prognostic significance of perioperative serum carcinoembryonic antigen in non-small cell lung cancer: analysis of 1,000 consecutive resections for clinical stage I disease. *Ann Thorac Surg*. 2004;78:216-21.
14. Okada M, Nishio W, Sakamoto T, Uchino K, Yuki T, Nakagawa A, et al. Effect of histologic type and smoking status on interpretation of serum carcinoembryonic antigen value in non-small cell lung carcinoma. *Ann Thorac Surg*. 2004;78:1004-9.
15. Boellaard R, Oyen WJG, Hoekstra CJ, Hoekstra OS, Visser EP, Willemsen AT, et al. The Netherlands protocol for standardisation and quantification of FDG whole body PET studies in multi-centre trials. *Eur J Nucl Med Mol Imaging*. 2008;35:2320-33.
16. Boellaard R, Krak NC, Hoekstra OS, Lammertsma AA. Effects of noise, image resolution, and ROI definition on the accuracy of standard uptake values: a simulation study. *J Nucl Med*. 2004;45:1519-27.
17. Westerterp M, Pruim J, Oyen W, Hoekstra O, Paans A, Visser E, et al. Quantification of FDG PET studies using standardized uptake values in multicenter trials: effects of image reconstruction, resolution and ROI definition parameters. *Eur J Nucl Med Mol Imaging*. 2007;34:392-404.

Published OnlineFirst December 21, 2011; DOI:10.1158/1078-0432.CCR-11-1946

Clinical Cancer Research

Upregulation of Notch2 and Six1 Is Associated with Progression of Early-Stage Lung Adenocarcinoma and a More Aggressive Phenotype at Advanced Stages

Takahiro Mimae, Morihito Okada, Man Hagiyama, et al.

Clin Cancer Res 2012;18:945-955. Published OnlineFirst December 21, 2011.

Published OnlineFirst December 21, 2011; DOI:10.1158/1078-0432.CCR-11-1946

Clinical Cancer Research

Human Cancer Biology

Upregulation of Notch2 and Six1 Is Associated with Progression of Early-Stage Lung Adenocarcinoma and a More Aggressive Phenotype at Advanced Stages

Takahiro Mimae[1,2], Morihito Okada[1], Man Hagiyama[2,3], Yoshihiro Miyata[1], Yasuhiro Tsutani[1], Takao Inoue[3], Yoshinori Murakami[2], and Akihiko Ito[3]

Abstract

Purpose: Lung adenocarcinoma often manifests as tumors with mainly lepidic growth. The size of invasive foci determines a diagnosis of *in situ*, minimally invasive adenocarcinoma, or invasive types and suggests that some adenocarcinomas undergo malignant progression in that order. This study investigates how transcriptional aberrations in adenocarcinoma cells at the early stage define the clinical phenotypes of adenocarcinoma tumors at the advanced stage.

Experimental Design: We comprehensively searched for differentially expressed genes between preinvasive and invasive cancer cells in one minimally invasive adenocarcinoma using laser capture microdissection and DNA microarrays. We screened expression of candidate genes in 11 minimally invasive adenocarcinomas by reverse transcriptase PCR and examined their involvement in preinvasive-to-invasive progression by transfection studies. We then immunohistochemically investigated the presence of candidate molecules in 64 samples of advanced adenocarcinoma and statistically analyzed the findings, together with clinicopathologic variables.

Results: The transcription factors *Notch2* and *Six1* were upregulated in invasive cancer cells in all 11 minimally invasive adenocarcinomas. Exogenous Notch2 transactivated *Six1* followed by *Smad3*, *Smad4*, and *vimentin*, and enlarged the nuclei of NCI-H441 lung epithelial cells. Immunochemical staining for the transcription factors was double positive in the invasive, but not in the lepidic growth component of a third of advanced Ads, and the disease-free survival rates were lower in such tumors.

Conclusions: Paired upregulation of *Notch2* and *Six1* is a transcriptional aberration that contributes to preinvasive-to-invasive adenocarcinoma progression by inducing epithelial–mesenchymal transition and nuclear atypia. This aberration persisted in a considerable subset of advanced adenocarcinoma and conferred a more malignant phenotype on the subset. *Clin Cancer Res; 18(4); 945–55. ©2011 AACR.*

Introduction

Adenocarcinoma is the most widespread histologic subtype of lung cancer in most countries, accounting for almost half of all lung cancers (1). Lung adenocarcinomas, especially advanced tumors, rarely comprise a single histologic component, and more than 90% of lung adenocarcinomas are of the mixed subtype according to the 2004 WHO classification (2). In an effort to address the complex histologic heterogeneity of adenocarcinomas, a new classification has recently been proposed (3). According to it, a small tumor with the lepidic growth pattern is diagnosed as either adenocarcinoma *in situ* or minimally invasive adenocarcinoma, depending on the presence or absence of microinvasion (≤ 5 mm). If a microinvasion focus of a minimally invasive adenocarcinoma becomes overt (overt invasion; > 5mm), the tumor will be then diagnosed as lepidic-predominant invasive adenocarcinoma. As might be predicted from these diagnostic criteria, to clearly distinguish between adenocarcinoma *in situ* and minimally invasive adenocarcinoma, as well as between minimally invasive adenocarcinoma and lepidic-predominant invasive adenocarcinoma can be difficult. Rather, it seems reasonable to consider that a significant subset of these 3 subtypes is biologically serial and that each subtype represents a different stage of adenocarcinoma progression.

The concept of progression from adenocarcinoma *in situ* to minimally invasive adenocarcinoma is widely accepted (4–9). Noguchi and colleagues noted 2 types of small

Authors' Affiliations: [1]Surgical Oncology, Division of Genome Radiobiology and Medicine, Programs for Biomedical Research, Graduate School of Biomedical Sciences, Hiroshima University, Hiroshima; [2]Division of Molecular Pathology, Institute of Medical Science, University of Tokyo, Tokyo; and [3]Department of Pathology, Faculty of Medicine, Kinki University, Osaka, Japan

Note: Supplementary data for this article are available at Clinical Cancer Research Online (http://clincancerres.aacrjournals.org/).

Corresponding Author: Akihiko Ito, Department of Pathology, Faculty of Medicine, Kinki University, 377-2 Ohno-Higashi, Osaka-Sayama, Osaka 589-8511, Japan. Phone: 81-72-366-0221; Fax: 81-72-360-2028; E-mail: aito@med.kindai.ac.jp

doi: 10.1158/1078-0432.CCR-11-1946

Published OnlineFirst December 21, 2011; DOI:10.1158/1078-0432.CCR-11-1946

Translational Relevance

Lung adenocarcinomas with mainly lepidic growth component are diagnosed as *in situ*, minimally invasive adenocarcinoma, or lepidic-predominant invasive adenocarcinoma types, depending on the size of invasive foci. In a minimally invasive adenocarcinoma, differentially expressed genes were comprehensively searched between the preinvasive and invasive components, and 2 transcriptional factors, *Notch2* and *Six1*, were identified as genes upregulated in the invasive component in all 11 minimally invasive adenocarcinomas examined. Transfection experiments suggested that Notch2 and Six1 cooperatively induced epithelial–mesenchymal transition of adenocarcinoma cells. Clinicopathologic analyses revealed that upregulation of both Notch2 and Six1 in invasive foci was detected in one-third of 64 lepidic-predominant invasive adenocarcinomas, and these tumors represented an aggressive phenotype. Paired upregulation of *Notch2* and *Six1* seemed to occur during preinvasive-to-invasive adenocarcinoma progression and define a more malignant subset of advanced adenocarcinoma. Notch2 and Six1 are not only useful biomarkers for malignant potential of adenocarcinoma but also can be therapeutic targets in adenocarcinoma.

(maximum diameter, < 2 cm) adenocarcinomas. These are type A (adenocarcinoma *in situ* according to the 2011 classification) that consists entirely of neoplastic cells that grow in lepidic growth pattern and type C (minimally invasive adenocarcinoma according to the 2011 classification) that consists of peripheral lepidic growth and a central microinvasion focus. The 2 types of tumors differ clinicopathologically. (i) After complete resection, patients with type A have 100% disease-specific survival, whereas the 5-year survival rate for patients with type C is 75% (9). (ii) Type C tumors have higher rates of p53 positivity, proliferation, and nuclear atypia than type A (8, 10, 11). Interpreting these data based on the 2011 classification, the microinvasion focus of minimally invasive adenocarcinoma is considered to develop due to the malignant progression of noninvasive, *in situ* neoplastic cells of the lepidic growth component. In contrast to the development of type C or minimally invasive adenocarcinoma tumors, the progression of minimally invasive adenocarcinoma to more advanced forms, including lepidic-predominant invasive adenocarcinoma, has not been studied in detail.

Genetic studies of adenocarcinoma progression have found mutations in *KRAS* and *EGFR* at the preinvasive stage, such as atypical adenomatous hyperplasia and adenocarcinoma *in situ* (12–15), and some adenocarcinomas have the amplification of these genes at the later stage of invasion and metastasis (7, 16, 17). Besides such genomic alterations, specific transcriptional pathways seem to become upregulated during the progression of adenocarcinoma, because recent findings have increasingly clarified that lung cancer progression is promoted by epithelial–mesenchymal transition (EMT; ref. 18) that is controlled by a group of transcription factors that includes Slug, which is a zinc finger type (19). The homeobox transcription factors Oct4 and downstream Nanog both function upstream of Slug to promote EMT in A549 lung adenocarcinoma cells (20). Although lung adenocarcinoma progression is assumed to be a stepwise process triggered by multiple genetic aberrations, which aberration(s) accounts for each process in the stepwise progression requires precise examination.

In this study, we attempted to obtain the genetic evidence, indicating that all or a subset of lepidic-predominant invasive adenocarcinoma develops from minimally invasive adenocarcinoma, and to clarify what clinical phenotypes the subset has. For this purpose, we designed the experiments that were composed of 3 parts. In the first part, we aimed to comprehensively compare the gene expression profiles between lepidic growth and microinvasion cancer cells from a single minimally invasive adenocarcinoma and successfully identified 2 transcription factors *Notch2* and *Six1* as genes upregulated in microinvasion cells. In the second part, we examined whether the identified genes might play causative roles in early-stage adenocarcinoma progression from lepidic growth to microinvasion cells, and found that Notch2 and Six1 coordinately induced EMT and nuclear atypia in lung epithelial cells. Finally in the third part, we immunohistochemically stained 64 specimens of lepidic-predominant invasive adenocarcinoma for Notch2 and Six1 and found that a third were a simple advanced form of minimally invasive adenocarcinoma, judging from the upregulation of Notch2 and Six1 in overt invasion cells. Importantly, the disease-free survival of patients with such tumors was poorer.

Materials and Methods

Sample selection

This study included patients with both consolidated lung tumors and ground glass opacities on chest high-resolution computed tomography images who underwent lobectomy or segmentectomy at Hiroshima University Hospital between 2007 and 2010 (Hiroshima, Japan). All patients provided written, informed consent to participate in this study and our Institutional Review Board approved the protocol (approval number: Hi-29). Half of the cancerous tissues were placed in Ultramount Aqueous Permanent Mounting Medium (DakoCytomation) and frozen for later studies, whereas the other half was preserved in 10% formalin for diagnosis. Gene expression was analyzed in samples of minimally invasive adenocarcinoma from 11 patients and 64 lepidic-predominant invasive adenocarcinoma tumor samples were immunohistochemically stained.

Cell culture

NCI-H441 human lung papillary adenocarcinoma cells, A549 human lung adenocarcinoma cells and MDA-MB-231

Published OnlineFirst December 21, 2011; DOI:10.1158/1078-0432.CCR-11-1946

human breast cancer cells were purchased from the American Type Culture Collection and RERF-LC-MS human lung adenocarcinoma cells were from Japanese Cancer Research Resources Bank (JCRB, Osaka, Japan) in 2010, and all experimentation using cell lines proceeded within 6 months after resuscitation. NCI-H441 cells and A549 cells were grown in RPMI-1640 (Nacalai Tesque) and Dulbecco's Modified Eagle Medium (Nacalai Tesque) supplemented with 10% FBS, antibiotics containing 100 units/mL penicillin, 100 μg/mL streptomycin (Invitrogen), and 0.01M-HEPES buffer (Nacalai Tesque) at 37°C in 5% CO_2/95% air. RERF-LC-MS cells were grown in Eagle's minimal essential medium (Nacalai Tesque) supplemented with 10% FBS, antibiotics, and 0.1 mmol/L nonessential amino acids (GIBCO-Invitrogen) at 37°C in 5% CO_2/95% air. MDA-MB-231 cells were grown in L-15 (Sigma-Aldrich) medium supplemented with 10% FBS, antibiotics, and 0.3 g/L L-glutamine (Sigma-Aldrich) at 37°C in 100% air.

Laser capture microdissection

Serial 15-μm sections of the 11 frozen minimally invasive adenocarcinoma tumors were stained with hematoxylin. Only cancer cells were selectively and separately collected from the lepidic growth and microinvasion components using laser capture microdissection (LMD7000; Leica Microsystems GmbH). The cancer cells were placed in the caps of collection tubes containing Tris [2-carboxyethyl] phosphine hydrochloride buffer. The collection time for one slide was 30 minutes. Twenty slides were done for each component. Each cell pool was frozen with dry ice immediately after collection.

RNA purification and amplification with Cy3 or Cy5 labeling

Total RNA was extracted from each cell pool using NucleoSpin RNA XS (Macherey-Nagel GmbH & Co. KG) and from one small ($\leq$ 1 cm) minimally invasive adenocarcinoma tumor and then cDNAs and amino allyl aRNA were synthesized from the RNA using Amino Allyl MessageAmp II aRNA Amplification Kits (Applied Biosystems). CyeDye coupling and fragmentation proceeded according to a protocol supplied by Toray Industries Inc. The concentration, purity, and integrity of the amplified and labeled aRNA were determined using a Eukaryotes Total RNA Nano Series II (Agilent Technologies). Total RNA from cultured cells was also extracted using NucleoSpin RNA XS.

Gene microarray analysis

Amplified RNA samples from microinvasion components were analyzed using 3D-Gene Human Oligo chip 25k (Toray Industries Inc.) microarrays of 25,370 distinct genes and RNA samples from lepidic growth components as controls. The 3-dimensional microarrays were constructed with wells as spaces between probes and cylinder stems with 70-mer oligonucleotide probes on the top to promote efficient hybridization. Cy3- or Cy5-labeled aRNA pools in hybridization buffer were hybridized for 16 hours according to the supplier's protocol (www.3d-gene.com). Hybridization signals were scanned using ScanArray Express Scanner (PerkinElmer) and processed using GenePixPro version 5.0 (Molecular Devices). Signals detected for each gene were normalized by global normalization (Cy3/Cy5 ratio median = 1) and Cy3/Cy5 normalized ratios >2.0 or <0.5 were, respectively, defined as commonly upregulated or downregulated genes.

Semiquantitative reverse transcriptase PCR

We analyzed the expression of *Notch2*, *Six1*, *thyroid transcription factor-1* (*TTF-1*), *Smad3*, *Smad4*, *vimentin*, *E-cadherin*, and *GAPDH* mRNA using reverse transcriptase PCR (RT-PCR) using SuperScriptTMIII First-Strand Synthesis SuperMix (Invitrogen) for the RT. In brief, total RNA was incubated with 50 ng of random hexamer primers and 1 μL of annealing buffer at 65°C for 5 minutes. The RNA was then incubated at 25°C for 5 minutes and at 50°C for 50 minutes in a final volume of 20 μL of reaction mixture containing 1× first-strand reaction mix comprising 5 mmol/L $MgCl_2$, 0.5 mmol/L of each deoxynucleotide triphosphate (dNTP), and 2 μL of SuperScriptTMIII/RNaseOUTTM Enzyme Mix.

The cDNA constructs were amplified by PCR using TaKaRa Ex Taq (Takara). The PCR conditions were 35 cycles of 30 seconds at 94°C (denaturation), 30 seconds at 55°C (annealing), and 30 seconds at 72°C (extension). The sense and antisense primers were 5′-AAAAATGGGGCCAACCGAGAC-3′ and 5′-TTCATCCAGAAGGCGCACAA-3′ for human *Notch2*, 5′-ACTCTCTGCTCGGCCCCCTC-3′ and 5′-AAGGCTGCTGAAACAGGCGT-3′ for human *Six1*, 5′-ATGTCGATGAGTCCAAAG-3′ and 5′-TCACCAGGTCCGA-3′ for human *TTF-1*, 5′-CGGGCCATGGAGCTGTGTGA-3′ and 5′-ACCTGCGTCCATGCTGTGGT-3′ for human *Smad3*, 5′-TCAGGGCCTCAGCCAGGACA-3′ and 5′-TCTCCTCCAGAAGGGTCCACGT-3′ for human *Smad4*, 5′-CAAGGGCCAAGGCAAGTCGC-3′ and 5′-GCCGTGAGGTCAGGCTTGGA-3′ for human *vimentin*, 5′-CCCTGGCTTTGACGCCGAGA-3′ and 5′-AAACGGAGGCCTGATGGGGC-3′ for human *E-cadherin*, and 5′-ACCACAGTCCATGCCATCAC-3′ and 5′-TCCACCACCCTGTTGCTGTA-3′ for human *GAPDH*, respectively. The PCR products were resolved by electrophoresis on 1% agarose gels, stained with ethidium bromide, and densitometrically analyzed. The RT-PCR signal intensity was quantified using ImageJ software (NIH) to compare *Notch2*, *Six1*, *TTF-1*, *Smad3*, *Smad4*, *vimentin*, *E-cadherin*, and *GAPDH* mRNA levels.

Construction of plasmid vectors expressing Notch2 intracellular domain, TTF-1, and siRNA against Six1

The cDNA construct for Notch2 intracellular domain (ICD; amino acids 1,703–2,475) inserts was amplified by PCR using KOD FX DNA polymerase (Toyobo Co. Ltd.) with following primer set: sense, 5′-CCGGATCCATGAAGCGTAAG-3′ (containing the first codon of Notch2 ICD); antisense, 5′-CCGTTAACTCACGCATAAACCTG-3′ (containing the stop codon of Notch2 ICD). The *TTF-1* gene produces 2 alternative transcripts, of which the short form consists of more than 90% of the total transcripts (21). The open reading frame of the short form of the cDNA from

NCI-H441 cells was amplified by PCR using the primer set: sense, 5′-CCGAATTCATGTCGATGAGTCCAAAG-3′; antisense, 5′-CCGTTAACTCACCAGGT-CCGA-3′. The PCR products were resolved by electrophoresis on 1% agarose gels and stained with ethidium bromide. Targeted bands were excised from gels and DNA was extracted and purified using the Wizard SV Gel and PCR Clean-Up System (Promega Corporation), as described by the manufacturer. Extracted DNA chains were annealed and ligated into the *Bam*HI/*Hpa*I (for Notch2) and *Eco*RI/*Hpa*I (for TTF-1) sites of pCX4-bsr, a modified pCX-bsr retroviral vector (22) provided by Dr. T. Akagi (Osaka Bioscience Institute, Osaka, Japan), and sequenced.

The pSilencer4.1-CMVneo siRNA plasmid vector (Ambion) was used to construct pSilencer4.1-CMVneo-si-Six1 and the negative control, pSilencer4.1-CMVneo-scramble. A DNA chain with the following sense and antisense sequences was synthesized to target the Six1 sequence: 5′-GATCCCCAGCTCAGAAGAGGAATTTTC-AAGAGAAA-TTCCTCTTCTGAGCTGGTT-3′ (sense) and 5′-AGCTTAACCAGCTCAGAAGAGGAATT-TCTCTTGAA-AATTCCTCTTCTGAGCTGGG-3′ (antisense). The target sequence of the negative control (scramble-pSilencer4.1-CMVneo) was 5′-GATCCCGT-CGATTTTGTGATGCTCG-TCAGTTCAAGAGACTGACGAGCATCACAAAATCGACG-G-TT-3′ (sense) and 5′-AGCTTAACGTCGATTTTGTGA-TGCTCGTCAGTCTCTTGAACTGA-CGAGCATCACAAAAT-CGACGG-3′ (antisense), which has no homology with any human DNA. The DNA chains were annealed and ligated into the *Bam*HI/*Hin*dIII sites of pSilencer4.1-CMVneo to generate pSilencer4.1-CMVneo-si-Six1. The negative control pSilencer4.1-CMVneo-scramble vector was constructed in the same manner. The plasmids were extracted and the accuracy of the constructs was confirmed by sequencing.

Transfection

NCI-H441 cells were transiently transfected with empty pCX4-bsr, pCX4-bsr-Notch2 ICD, or pCX4-bsr-TTF-1 using FuGENE 6 (Roche Applied Science). In brief, 2.0×10^5 cells were seeded on 60-mm culture dishes overnight until 50% to 80% confluence was reached. Serum-free medium (194 μL) and 6.0 μL of FuGENE 6 reagent were mixed in 1.5-mL tubes and incubated for 5 minutes at room temperature. Plasmid vectors (2.0 μg each) were added and the contents were mixed and incubated with transfection reagent and DNA complex for at least 15 minutes at room temperature. The transfection reagent and DNA complex were added drop wise to the cultured cells and incubated for 48 hours. The medium was removed and the cells were rinsed 3 times with PBS. The transfected cells were then used in various experiments. A549, RERF-LC-MS, and MDA-MB-231 were also transiently transfected with empty pCX4-bsr or pCX4-bsr-Notch2 ICD using FuGENE 6.

Double transfection proceeded as follows. NCI-H441 cells were transiently transfected with 2.0 μg of each of pCX4-bsr-Notch2 ICD and the empty pSilencer4.1-CMVneo, or pSilencer4.1-CMVneo-scramble, or pSilencer4.1-CMVneo -si-Six1 using FuGENE 6.

Immunohistochemistry

Tissues fixed with 10% formalin were embedded in paraffin and cut into 4-μm thick sections that were deparaffinized, rehydrated, and autoclaved for 20 minutes at 121°C in 10 mmol/L citrate buffer (pH 6.0) and then incubated in methanol containing 3% peroxide for 5 minutes. The sections were washed 3 times with PBS between all steps of the procedure. Nonspecific Ig binding in the sections was blocked by incubation with PBS containing 2% bovine serum albumin (BSA) for 10 minutes. The sections were then incubated with anti-Notch2 antibody (ab8926, 1:400 dilution; Abcam) and/or anti-Six1 antibody (HPA001893, 1:100 dilution; Sigma-Aldrich) in PBS containing 2% BSA for 2 hours at room temperature, followed by horseradish peroxidase–conjugated anti-rabbit Ig G antibody (1:100 dilution; Santa Cruz) in PBS containing 2% BSA for 2 hours at 4°C. Color was developed using aminoethylcarbazole (DAB; Dako) as the substrate for peroxidase. Tissues were counterstained with hematoxylin and mounted. Negative immunohistochemical control procedures comprised the omission and replacement of primary antibodies with appropriate concentrations of normal rabbit or mouse IgG. Slides were examined using a light microscope (BX51; Olympus) equipped with a CCD camera DP72 (Olympus). The results on the control slides were negative.

Cancer cells were deemed positive for Notch2 when the cytoplasm of over half of the cancer cells in each of the lepidic growth and microinvasion components was intensely stained. Other staining profiles were defined as negative. Cancer cells were deemed positive for Six1 when nuclei in over half of the cancer cells in each of the lepidic growth and microinvasion components were intensely stained. Other staining profiles were defined as negative.

Nuclear size analysis

Five minimally invasive adenocarcinoma tumors that contained a Notch2-negative lepidic growth component and a Notch2-positive microinvasion component were immunohistochemically selected. The greatest nuclear dimension of cancer cells in both the lepidic growth and microinvasion components was separately determined in 5 tumors using hematoxylin and eosin (H&E) staining and light microscopy (BX51). The greatest nuclear dimension of 200 cells was measured in random fields for each component from each tumor. The greatest nuclear dimension of the control and of NCI-H441 cells transfected *in vitro* with empty pCX4-bsr, pCX4-bsr-Notch2 ICD, or pCX4-bsr-TTF-1 was assessed by nuclear staining using 4′,6-diamino-2-phenylindole (DAPI) and the fluorescence microscope, Axio Observer D1 (Carl Zeiss). We determined the nuclear dimensions of 100 cells in randomly selected fields in 3 independent experiments.

Statistical analysis

Data about signal intensity and cell morphology are described as means ± SD or as means ± SE and were analyzed using Student *t* test. The clinicopathologic findings were analyzed using the Mann–Whitney *U* test for

Published OnlineFirst December 21, 2011; DOI:10.1158/1078-0432.CCR-11-1946

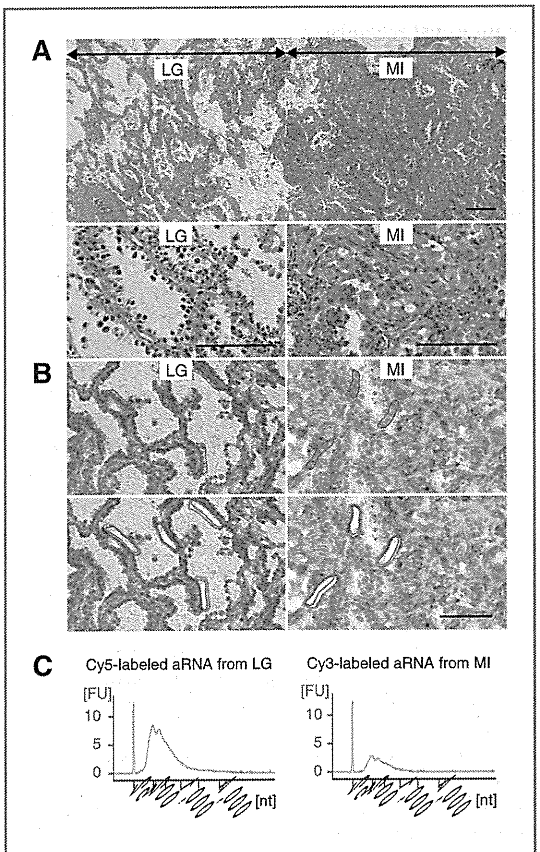

Figure 1. Laser capture microdissection of lepidic growth (LG) and microinvasion (MI) cancer cells from a single minimally invasive adenocarcinoma (case 1) and probe preparation for DNA microarray analysis. A, photomicrograph of minimally invasive adenocarcinoma from case 1 stained with H&E. Top, low-power field view (original magnification, ×100) containing both lepidic growth and microinvasion components; bottom, high-power field view (original magnification, ×400) of each component. B, lepidic growth and microinvasion cancer cells collected by laser capture microdissection from frozen sections of minimally invasive adenocarcinoma tumor. Cancer cells circled in red (top) were cut out using laser pulses run along the circles (bottom). C, verification of aRNA probes for DNA microarray analysis. Total RNA extracted from pools of lepidic growth and microinvasion cancer cells served as templates for preparation of aRNA probes. Quality and quantities of probes were verified by resolving Cy3- or Cy5-labeled aRNA by capillary gel electrophoresis. The amounts of RNA extracted and amplified were 46.2 ng and 14.3 μg for lepidic growth component and 48.4 ng and 4.0 μg for microinvasion component, respectively. Bar, 100 μm.

continuous variables and χ^2 tests for categorical variables. Disease-free survival (DFS) curves were calculated using the Kaplan–Meier method. Univariate and multivariate analyses were done using the log-rank and logistic regression tests, respectively. A P value of ≤ 0.05 was regarded as significant.

Results

Isolation of genes that are differentially expressed in lepidic growth and microinvasion cancer cells in a single minimally invasive adenocarcinoma

A small (1 cm in greatest dimension), solitary lung tumor was surgically resected and histopathologically diagnosed as minimally invasive adenocarcinoma (formerly, type C by Noguchi classification; Fig. 1A; case 1 in Fig. 2A and Supplementary Table S1). We separately isolated lepidic growth and microinvasion cancer cells without contamination from frozen tumor sections using a laser capture microdissection system (Fig. 1B). We extracted total RNAs from about 500 lepidic growth and microinvasion cancer cells and then amplified and labeled the RNAs using T7 RNA polymerase. Fig. 1C shows the amounts and quality of the original total RNAs and amplified aRNAs. The aRNAs were comparatively analyzed using highly sensitive oligo DNA microarrays. The complete gene expression dataset of the microdissected minimally invasive adenocarcinoma specimen is available at Gene Expression Omnibus (GEO) accession number GSE30663 (23). The numbers of genes whose expression levels were double or more and half or less in the microinvasion cancer cells were 2,905 and 2,143, respectively. Supplementary Table S2 shows the top 30 of each of

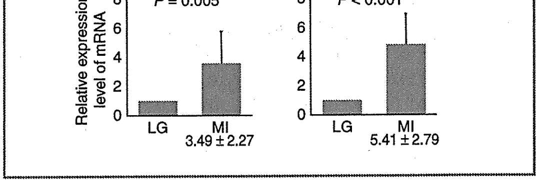

Figure 2. RT-PCR analyses of *Notch2* and *Six1* in total RNA from lepidic growth (LG) and microinvasion (MI) cancer cells in 11 minimally invasive adenocarcinomas. lepidic growth and microinvasion cancer cells were separately collected from frozen sections of minimally invasive adenocarcinomas (cases 1 to 11 listed in Supplementary Table S1) using laser capture microdissection. Total RNAs were extracted from each cell pool and analyzed by RT-PCR using primer sets for *Notch2*, *Six1*, or *GAPDH*. Portions of PCR products were resolved by electrophoresis on 1% agarose gels (A). All band intensities were converted to densitometric values; *Notch2* and *Six1* values were normalized to that of *GAPDH* and then means and SD of 11 minimally invasive adenocarcinomas were calculated. Expression levels of *Notch2* and *Six1* mRNA in microinvasion cancer cells are expressed as relative values normalized to 1 for means in lepidic growth cancer cells (B).

Published OnlineFirst December 21, 2011; DOI:10.1158/1078-0432.CCR-11-1946

the upregulated (>94-fold) and downregulated (<1/25.4-fold) candidate genes.

Upregulation of Notch2 and its downstream Six1 in microinvasion cancer cells

We found that *Six1* (136-fold) was the most upregulated among the top 30 genes in microinvasion cancer cells, and *Notch2* was 10.7-fold upregulated in the complete dataset. We considered that this paired upregulation was worthy of further investigation because both Six1 and Notch2 can function as transcription factors and Six1 is a putative downstream target of Notch2 (24, 25). As with minimally invasive adenocarcinoma from case 1, we extracted total RNAs from lepidic growth and microinvasion cancer cells separately from minimally invasive adenocarcinomas resected from cases 2 to 11 (Fig. 2A and Supplementary Table S1). *Six1* and *Notch2* mRNA expression was then screened in all 11 minimally invasive adenocarcinomas by semiquantitative RT-PCR. Significantly more mRNA for either gene was found in microinvasion than in lepidic growth cancer cells from all 11 minimally invasive adenocarcinomas (Fig. 2A and B). The expression of Notch2 and Six1 proteins was examined in the case 10 minimally invasive adenocarcinoma by immunohistochemistry. Notch2 and Six1 immunoreactive signals were clearly detected in the cytoplasm and nucleus of microinvasion cancer cells, respectively, whereas lepidic growth component cells were nearly completely negative for the two molecules (Fig. 3).

We speculated whether Notch2 upregulation results in *Six1* transactivation in lung epithelial cells and examined this notion in NCI-H441 cells that have been widely studied as lung epithelial cells. The results of RT-PCR analyses revealed that these cells expressed endogenously undetectable levels of *Notch2* or *Six1* (Fig. 4A, lane 1). Because Notch2 is enzymatically processed to release its ICD that functions as a transcription factor (26), we subcloned Notch2 ICD cDNA into the mammalian expression vector, pCX4-bsr. NCI-H441 cells transfected with this plasmid contained not only abundant exogenous transcripts for Notch2 ICD but also abundant endogenous transcripts for Six1 (Fig. 4A, lane 3 and Supplementary Fig. S1). We also transfected NCI-H441 cells with the cDNA for TTF-1, well known as a lung epithelial transcription factor, but *Six1* transactivation was undetectable (Fig. 4A, lane 4 and Supplementary Fig. S1). Similar experiments using MDA-MB-231 breast cancer cells that express endogenously detectable levels of *Notch2* and *Six1* showed that exogenous Notch2 ICD did not upregulate, but rather slightly downregulated *Six1* (Fig. 4A, lanes 8–10). These results suggested that Notch2 specifically transactivates *Six1* in NCI-H441.

Involvement of Notch2 and Six1 in EMT and nuclear atypism in lung epithelial cells

Notch2 and Six1 promote EMT in various cancers partly through activating the TGF-β intracellular signaling pathways that involve the intracellular signal transducers Smad3 and Smad4 (27–29). Consistent with their epithelioid morphology, NCI-H441 cells expressed easily and faintly detectable levels of *E-cadherin* and *vimentin*, respectively (Fig. 4A, lane 1). The expression levels of these two genes were inverse in NCI-H441 cells transfected with Notch2 ICD cDNA (Fig. 4A, lane 3 and Supplementary Fig. S2). Such transfection also resulted in *Smad3* and *Smad4* transactivation (Fig. 4A, lane 3 and Supplementary Fig. S2). Transfection with the empty vector did not alter the endogenous expression of these 4 genes (Fig. 4A, lane 2 and Supplementary Fig. S2). Transfection with TTF-1 resulted in *vimentin* transactivation and *E-cadherin* downregulation (Fig. 4A, lane 4 and Supplementary Fig. S2). Notch2 seemed to promote EMT in NCI-H441 cells more efficiently than TTF-1. NCI-H441 cells were transfected with Notch2 ICD cDNA and with either Six1-targeting siRNA or a control scrambled siRNA. The Six1-targeting siRNA abrogated not only Notch2 ICD–induced transactivation of *Six1* but also

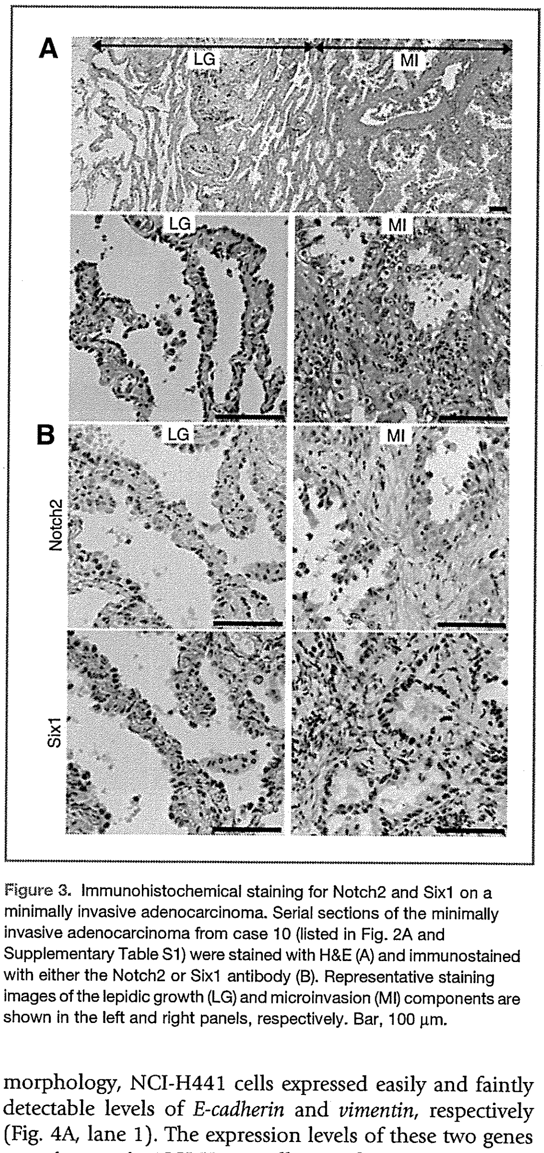

Figure 3. Immunohistochemical staining for Notch2 and Six1 on a minimally invasive adenocarcinoma. Serial sections of the minimally invasive adenocarcinoma from case 10 (listed in Fig. 2A and Supplementary Table S1) were stained with H&E (A) and immunostained with either the Notch2 or Six1 antibody (B). Representative staining images of the lepidic growth (LG) and microinvasion (MI) components are shown in the left and right panels, respectively. Bar, 100 μm.

Published OnlineFirst December 21, 2011; DOI:10.1158/1078-0432.CCR-11-1946

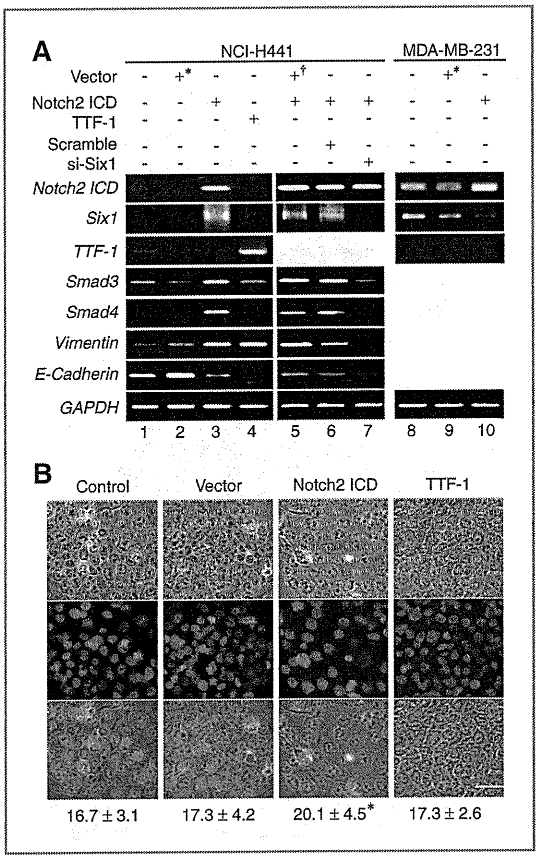

Figure 4. Transcriptional and cell morphologic alterations induced by exogenous Notch2 ICD in NCI-H441 cells. A, expression of EMT-related genes in NCI-H441 and MDA-MB-231 cells before and after transfection with various transcription factors and si-RNA. NCI-H441 and MDA-MB-231 cells were transiently transfected with pCX4-bsr empty (*lanes 2 and 9) or with vectors expressing either Notch2 ICD (lanes 3 and 10) or TTF-1 (lane 4). NCI-H441 cells were transiently transfected in some experiments with Notch2 ICD cDNA and with either empty pSilencer4.1-CMVneo (†lane 5) or vectors expressing scrambled (lane 6) or Six1-targeting (lane 7) siRNA. Total RNAs extracted from intact or transfected cells were analyzed by RT-PCR using primer set for indicated genes. Portions of PCR products were resolved by electrophoresis on 1% agarose gels. B, changes in sizes of nuclei in NCI-H441 cells transfected with Notch2 ICD cDNA. NCI-H441 cells were transfected or not (control) with either empty pCX4-bsr or vectors expressing cDNAs for Notch2 ICD or TTF-1 and then stained with DAPI to visualize nuclei (blue). Phase-contrast (top) and UV laser (middle) images of cells are merged (bottom). Sizes of nuclei were determined as described in Materials and Methods, and calculated means and SE are shown below the images. *, $P < 0.01$ compared with values of other types of cells. Bar, 50 μm.

that of *Smad3*, *Smad4*, and *vimentin*, whereas it further enhanced the Notch2 ICD–induced downregulation of *E-cadherin* (Fig. 4A, lane 7). Control transfection did not alter the gene expression induced by Notch2 ICD (Fig. 4A, lanes 5 and 6). These results indicated that Six1 is essential for Notch2 to transactivate *Smad3*, *Smad4*, and *vimentin*, but not to downregulate *E-cadherin*.

Notch2 ICD transfection experiments, followed by RT-PCR, were conducted on 2 other lung adenocarcinoma cell lines, A549 and RERF-LC-MS, both of which expressed endogenously undetectable levels of Notch2 and Six1 (Supplementary Fig. S3). Exogenous Notch2 ICD in these cells induced gene expression alterations resembling those in NCI-H441 cells, except that *Smad4* and *E-cadherin* were not upregulated in A549 and RERF-LC-MS, respectively (Supplementary Fig. S3). These results suggested that Notch2 and Six1 played pivotal roles in inducing EMT of lung adenocarcinoma cells.

Early-stage lung adenocarcinoma progression is assumed to be associated with an increase in the size of cancer cell nuclei (8). We measured the greatest dimension of cancer cell nuclei in 5 minimally invasive adenocarcinomas and found significantly larger nuclei in microinvasion, than in lepidic growth cancer cells from all 5 minimally invasive adenocarcinomas (Supplementary Table S1). A comparison between intact NCI-H441 cells and those transfected with the Notch2 ICD cDNA showed significantly larger nuclei in the transfectants than in the intact cells (Fig. 4B). Transfection with empty vector or with TTF-1 cDNA did not alter the size of nuclei in NCI-H441 cells (Fig. 4B).

Upregulation of Notch2 and Six1 defines a clinically aggressive phenotype of lepidic-predominant invasive adenocarcinoma

We immunohistochemically analyzed 64 samples of lepidic-predominant invasive adenocarcinoma tumors using antibodies against Notch2 and Six1. Table 1 summarizes the clinicopathologic features of each case. The immunohistochemical staining results were judged positive when more than 50% of the cancer cells in each of the lepidic growth and overt invasion components had significant cytoplasmic (Notch2) or nuclear (Six1) staining. The tumors were classified based this judgment as double (Notch2 and Six1) negative in lepidic growth, but double positive in overt invasion (N/P; $n = 23$) cells; double negative in both components (N/N; $n = 19$); double positive in both components (P/P; $n = 19$) and other ($n = 3$; summarized in Table 1). A representative staining profile of N/P tumors was shown in Supplementary Fig. S4. A statistical analysis of the clinicopathologic parameters among the groups showed that the N/P group was less favorable than the N/N group with respect to pT, pN, PL factor, and ly factor (Table 1). Univariate log-rank analyses of Kaplan–Meier survival curves revealed that DFS duration was shorter in the N/P, than in the N/N group ($P = 0.015$; Fig. 5). DFS duration was also affected by various clinicopathologic parameters including pStage, pT, pN, PL factor, and ly factor (Supplementary Table S3). Multivariate logistic regression analyses among the 3 groups revealed that the N/P and P/P groups were more likely to recur than the N/N group in 2-year postoperative follow-up (Supplementary Table S4).

Published OnlineFirst December 21, 2011; DOI:10.1158/1078-0432.CCR-11-1946

Table 1. Classification of patients with lepidic-predominant invasive adenocarcinoma according to Notch2 and Six1 immunohistochemical findings

Variable	All patients	Notch2 and Six1					
		N/N	N/P	P/P	Other		P
Sex						N/N vs. N/P	0.59
Male	36	10	14	11	1	N/N vs. P/P	0.74
Female	28	9	9	8	2	N/P vs. P/P	0.85
Age						N/N vs. N/P	0.95
Mean	71	70.5	70.7	70.8	78.3	N/N vs. P/P	0.93
Range	49–86	49–86	58–83	56–85	74–85	N/P vs. P/P	0.97
pStage[a]						N/N vs. N/P	0.33
IA + IB	52	17	18	14	3	N/N vs. P/P	0.21
IIA + IIB + IIIA + IIIB	12	2	5	5	0	N/P vs. P/P	0.73
pT[a]						N/N vs. N/P	0.04
1a + 1b	39	15	11	11	2	N/N vs. P/P	0.16
2a + 2b + 3	25	4	12	8	1	N/P vs. P/P	0.52
pN[a]						N/N vs. N/P	0.03
0	55	19	18	15	3	N/N vs. P/P	0.03
1 + 2	9	0	5	4	0	N/P vs. P/P	0.96
PL factor[a]						N/N vs. N/P	0.005
0	50	18	13	17	2	N/N vs. P/P	0.55
≥1	14	1	10	2	1	N/P vs. P/P	0.02
ly Factor[a]						N/N vs. N/P	0.039
0	46	18	16	10	2	N/N vs. P/P	0.003
1	18	1	7	9	1	N/P vs. P/P	0.26
v Factor[a]						N/N vs. N/P	0.67
0	56	18	21	14	3	N/N vs. P/P	0.08
1	8	1	2	5	0	N/P vs. P/P	0.13
Tumor size (mm)						N/N vs. N/P	0.89
Mean	25.3	25.5	25	24.7	30	N/N vs. P/P	0.82
Range	11–70	11–70	15–40	12–38	15–50	N/P vs. P/P	0.87

[a]According to TNM classification (7th Edition).

Discussion

This study comprised 3 parts. A clinical issue had to be considered for the first part that compared comprehensive gene expression between lepidic growth and microinvasion cancer cells in individual minimally invasive adenocarcinomas. Because the cut surface at the greatest dimension of the tumor is used for pathologic diagnosis, remaining specimens for LMD contained only a small amount of each component, particularly the microinvasion component. The original estimated amount of total RNA used for the present DNA microarray analysis was in the order of 100 ng per component or less. This limitation might have caused considerable RNA degradation and consequently resulting in shorter aRNA probes (theoretical average length, ~1.5 kb) (Fig. 1C). Regardless, the DNA microarray analysis seemed reliable because (i) the range of the relative expression levels of 10 housekeeping genes was sufficiently small

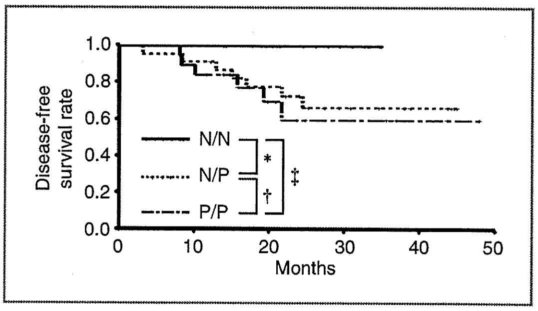

Figure 5. DFS rates of 64 lepidic-predominant invasive adenocarcinomas grouped by Notch2 and Six1 immunohistochemistry. DFS rates of N/N, N/P, and P/P tumor groups shown as function of months. The mean interval of DFS (95% CI) for N/P and P/P are 34.9 (28.8–41.1) months and 34.7 (26.2–43.2) months, respectively. Values for N/N were not calculated because N/N tumors did not recur. *, $P = 0.015$; †, $P = 0.626$; ‡, $P = 0.006$.

Published OnlineFirst December 21, 2011; DOI:10.1158/1078-0432.CCR-11-1946

(within 0.5- to 2-fold) between lepidic growth and microinvasion cells (Supplementary Table S2), and (ii) differential expression of the selected 2 genes, that is, *Notch2* and *Six1* genes, was reproducibly confirmed by RT-PCR (Fig. 2A, case 1). These results indicate that tumor lesions at the early stage that contain cancer cells with different malignant potential, for example, *in situ* and invasive cells in minimally invasive adenocarcinoma, are practical for comparative gene expression analyses among cancer cells during progression *in vivo*.

Both *Notch2* and *Six1* were upregulated in microinvasion cancer cells not only in the minimally invasive adenocarcinoma that was analyzed using DNA microarrays but also in 10 other minimally invasive adenocarcinomas examined. We therefore considered that paired upregulation of Notch2 and Six1 is commonly associated with the progression of lepidic growth to microinvasion cancer cells in minimally invasive adenocarcinoma. Notch2 is a cell membrane–bound ligand-dependent receptor for the Type 1 transmembrane protein family named Notch (30–33). When Notch ligands bind to Notch2 receptors between two neighboring cells, Notch2 is cleaved through a cascade of proteolytic enzymes, including γ-secretase, and released Notch2 ICD translocates into the nucleus where it transcriptionally activates Notch2 target genes (26). Although Notch1 and Notch3, other members of the Notch family, have long been regarded as candidate molecules responsible for the development of lung cancer (34–36), whether Notch2 has similar roles remains to be determined. Six1 is a homeodomain transcription factor (37) and a putative downstream target of Notch2 (24, 25). Interestingly, Ford and colleagues showed that Six1 stimulates the malignant transformation of mammary epithelial cells through transactivating *cyclin A1* (38, 39) and induces EMT in mammary cancer cells through the induction of TGF-β signaling (27, 40). These findings suggested that Notch2 and Six1 play coordinate roles during the early-stage lung adenocarcinoma progression.

The second part of this study examined this notion using transfection experiments. Consistent with previous characterization, exogenous expression of the Notch2 ICD resulted in *Six1* transactivation in NCI-H441 lung epithelial cells. The exogenous Notch2 ICD also transactivated *Smad3*, *Smad4*, and *vimentin* in association with the downregulation of *E-cadherin*. Similar transactivation effects of Notch2 ICD were detected in 2 other types of epithelial cells derived from lung adenocarcinomas. Interestingly, Six1 was notably essential for transactivation of the 3 genes, but not for the downregulation of *E-cadherin*, suggesting that Notch2 and Six1 coordinately played a causative role in inducing EMT during the progression of lepidic growth to microinvasion cells. Exogenous expression of the Notch2 ICD in NCI-H441 cells also resulted in nuclei becoming enlarged. This was in accordance with the cytologic finding that nuclei were larger in microinvasion cancer cells than in lepidic growth cells from 5 minimally invasive adenocarcinomas examined. These results supported the notion that the transcriptional cascades activated coordinately by Notch2 and Six1 are involved in lepidic growth-to-microinvasion progression.

The third part of the study immunohistochemically investigated Notch2 and Six1 in 64 samples of lepidic-predominant invasive adenocarcinoma tumors and found that they could be assigned almost equally into groups on the basis of positive and negative staining as N/N, N/P, and P/P. Consistent with the results of the second part of the study showing that Six1 is a downstream target of Notch2, these transcription factors were either double negative or double positive in lepidic growth and overt invasion cancer cells, respectively, with some exceptions. As might be predicted from the diagnostic criteria, lepidic-predominant invasive adenocarcinoma seemed to include heterogeneous tumors with distinct natural histories and genetic alterations. Judging from the immunostaining profiles of lepidic growth and overt invasion cells, N/P tumors seem to be a simple advanced form of minimally invasive adenocarcinoma, in which microinvasion cells have grown into an overt invasion focus, and N/N tumors develop via other molecular mechanisms than those involving Notch2 and Six1. On the other hand, the origin of P/P tumors is uncertain, but they might be a more advanced form of N/P tumors. Because lepidic growth cancer cells were positive for both Notch2 and Six1, they might be potentially invasive. This speculation is reminiscent of a recent report by Anami and colleagues who notably pointed out that the lepidic growth pattern might represent the intraalveolar epithelial spread of overt invasion cancer cells (41). Whether or not lepidic growth cancer cells are invasive did not seem to affect the prognostic outcomes of patients with lepidic-predominant invasive adenocarcinomas (N/P vs. P/P in Fig. 5). Interestingly, we found that N/N tumors metastasized less often to lymph nodes, were less invasive to lymphatic vessels, and were associated with better DFS than N/P and P/P tumors ($P = 0.015$ and 0.006 by log-rank tests, respectively). These findings agree with a summary of reviews that emphasize the critical role of Notch signals in the malignant progression of non-small cell lung cancer (34–36). The paired upregulation of Notch2 and Six1 seemed to be one transcriptional alteration that is responsible for minimally invasive adenocarcinoma-to-lepidic-predominant invasive adenocarcinoma progression, and it defined a clinically aggressive phenotype subset of lepidic-predominant invasive adenocarcinoma. Because Notch2 and Six1 immunohistochemistry seemed to independently discriminate lepidic-predominant invasive adenocarcinomas with high risk of recurrence in a 2-year postoperative period, during which the recurrence of most lung cancers occurs even after curative-intent therapy (42), it could be a clinically useful examination for selecting patients with lepidic-predominant invasive adenocarcinoma needing intensive follow-up.

Aviel-Ronen and colleagues (2008) examined genomic changes associated with adenocarcinoma *in situ* and minimally invasive adenocarcinoma using array comparative

Published OnlineFirst December 21, 2011; DOI:10.1158/1078-0432.CCR-11-1946

genomic hybridization and found that genomic profiles are indistinguishable between adenocarcinoma *in situ* and minimally invasive adenocarcinoma, although they developed in distinct individuals (5). In contrast, this study successfully revealed that gene expression profiles substantially differed between lepidic growth and microinvasion cancer cells in a single minimally invasive adenocarcinoma. The findings of these two studies and the present results indicate that the Notch2 and Six1 upregulation detected in minimally invasive adenocarcinoma is attributable not to particular genomic alterations, but to environmental factors, including immune and stromal cells around cancer cells. In fact, activation of the Notch2 signaling pathway is cell membrane–bound ligand dependent (26). Although further characterization of lepidic-predominant invasive adenocarcinoma is required at the molecular level, subclassification of lepidic-predominant invasive adenocarcinoma on the basis of Notch2 and Six1 upregulation seems to be clinically important in predicting the prognostic outcomes of patients with lepidic-predominant invasive adenocarcinoma.

Disclosure of Potential Conflicts of Interest

No potential conflicts of interest were disclosed.

Grant Support

This study was supported by grants from the Ministry of Education, Culture, Sports, Science and Technology of Japan and from the Nakatani Foundation of Electronic Measuring Technology Advancement.

The costs of publication of this article were defrayed in part by the payment of page charges. This article must therefore be hereby marked *advertisement* in accordance with 18 U.S.C. Section 1734 solely to indicate this fact.

Received July 28, 2011; revised December 14, 2011; accepted December 16, 2011; published OnlineFirst December 21, 2011.

References

1. Devesa SS, Bray F, Vizcaino AP, Parkin DM. International lung cancer trends by histologic type: male:female differences diminishing and adenocarcinoma rates rising. Int J Cancer 2005;117:294–9.
2. Motoi N, Szoke J, Riely GJ, Seshan VE, Kris MG, Rusch VW, et al. Lung adenocarcinoma: modification of the 2004 WHO mixed subtype to include the major histologic subtype suggests correlations between papillary and micropapillary adenocarcinoma subtypes, EGFR mutations and gene expression analysis. Am J Surg Pathol 2008;32:810–27.
3. Travis WD, Brambilla E, Noguchi M, Nicholson AG, Geisinger KR, Yatabe Y, et al. International association for the study of lung cancer/American Thoracic Society/European Respiratory Society international multidisciplinary classification of lung adenocarcinoma. J Thorac Oncol 2011;6:244–85.
4. Aoyagi Y, Yokose T, Minami Y, Ochiai A, Iijima T, Morishita Y, et al. Accumulation of losses of heterozygosity and multistep carcinogenesis in pulmonary adenocarcinoma. Cancer Res 2001;61:7950–4.
5. Aviel-Ronen S, Coe BP, Lau SK, da Cunha Santos G, Zhu CQ, Strumpf D, et al. Genomic markers for malignant progression in pulmonary adenocarcinoma with bronchioloalveolar features. Proc Natl Acad Sci U S A 2008;105:10155–60.
6. Seki N, Takasu T, Mandai K, Nakata M, Saeki H, Heike Y, et al. Expression of eukaryotic initiation factor 4E in atypical adenomatous hyperplasia and adenocarcinoma of the human peripheral lung. Clin Cancer Res 2002;8:3046–53.
7. Soh J, Toyooka S, Ichihara S, Asano H, Kobayashi N, Suehisa H, et al. Sequential molecular changes during multistage pathogenesis of small peripheral adenocarcinomas of the lung. J Thorac Oncol 2008;3:340–7.
8. Morishita Y, Fukasawa M, Takeuchi M, Inadome Y, Matsuno Y, Noguchi M. Small-sized adenocarcinoma of the lung. Cytologic characteristics and clinical behavior. Cancer 2001;93:124–31.
9. Noguchi M, Morikawa A, Kawasaki M, Matsuno Y, Yamada T, Hirohashi S, et al. Small adenocarcinoma of the lung. Histologic characteristics and prognosis. Cancer 1995;75:2844–52.
10. Maezawa N, Tsuta K, Shibuki Y, Yamazaki S, Maeshima AM, Watanabe S, et al. Cytopathologic factors can predict invasion in small-sized peripheral lung adenocarcinoma with a bronchioloalveolar carcinoma component. Cancer 2006;108:488–93.
11. Terasaki H, Niki T, Matsuno Y, Yamada T, Maeshima A, Asamura H, et al. Lung adenocarcinoma with mixed bronchioloalveolar and invasive components: clinicopathological features, subclassification by extent of invasive foci, and immunohistochemical characterization. Am J Surg Pathol 2003;27:937–51.
12. Lynch TJ, Bell DW, Sordella R, Gurubhagavatula S, Okimoto RA, Brannigan BW, et al. Activating mutations in the epidermal growth factor receptor underlying responsiveness of non-small-cell lung cancer to gefitinib. N Engl J Med 2004;350:2129–39.
13. Paez JG, Janne PA, Lee JC, Tracy S, Greulich H, Gabriel S, et al. EGFR mutations in lung cancer: correlation with clinical response to gefitinib therapy. Science 2004;304:1497–500.
14. Sakamoto H, Shimizu J, Horio Y, Ueda R, Takahashi T, Mitsudomi T, et al. Disproportionate representation of KRAS gene mutation in atypical adenomatous hyperplasia, but even distribution of EGFR gene mutation from preinvasive to invasive adenocarcinomas. J Pathol 2007;212:287–94.
15. Westra WH, Baas IO, Hruban RH, Askin FB, Wilson K, Offerhaus GJ, et al. K-ras oncogene activation in atypical alveolar hyperplasias of the human lung. Cancer Res 1996;56:2224–8.
16. Yatabe Y, Takahashi T, Mitsudomi T. Epidermal growth factor receptor gene amplification is acquired in association with tumor progression of EGFR-mutated lung cancer. Cancer Res 2008;68: 2106–11.
17. Tang ZQ, Han LY, Lin HH, Cui J, Jia J, Low BC, et al. Derivation of stable microarray cancer-differentiating signatures using consensus scoring of multiple random sampling and gene-ranking consistency evaluation. Cancer Res 2007;67:9996–10003.
18. Zhang HJ, Wang HY, Zhang HT, Su JM, Zhu J, Wang HB, et al. Transforming growth factor-beta1 promotes lung adenocarcinoma invasion and metastasis by epithelial-to-mesenchymal transition. Mol Cell Biochem 2011;355:309–14.
19. Shih JY, Yang PC. The EMT regulator slug and lung carcinogenesis. Carcinogenesis 2011;32:1299–304.
20. Chiou SH, Wang ML, Chou YT, Chen CJ, Hong CF, Hsieh WJ, et al. Coexpression of Oct4 and Nanog enhances malignancy in lung adenocarcinoma by inducing cancer stem cell-like properties and epithelial-mesenchymal transdifferentiation. Cancer Res 2010;70: 10433–44.
21. Li C, Cai J, Pan Q, Minoo P. Two functionally distinct forms of NKX2.1 protein are expressed in the pulmonary epithelium. Biochem Biophys Res Commun 2000;270:462–8.
22. Akagi T, Murata K, Shishido T, Hanafusa H. v-Crk activates the phosphoinositide 3-kinase/AKT pathway by utilizing focal adhesion kinase and H-Ras. Mol Cell Biol 2002;22:7015–23.
23. GEO Browser [Internet]. Bethesda (MD): National Library of Medicine (US); 2002. Expression profiling by array [cited 2011 Jul 14]. Available from: http://www.ncbi.nlm.nih.gov/geo/query/acc.cgi?token=plkbnogawiamexw&acc=GSE30663 Accession Number: GSE30663.

Published OnlineFirst December 21, 2011; DOI:10.1158/1078-0432.CCR-11-1946

24. Bessarab DA, Chong SW, Korzh V. Expression of zebrafish six1 during sensory organ development and myogenesis. Dev Dyn 2004;230:781–6.
25. Rodriguez S, Sickles HM, Deleonardis C, Alcaraz A, Gridley T, Lin DM. Notch2 is required for maintaining sustentacular cell function in the adult mouse main olfactory epithelium. Dev Biol 2008;314:40–58.
26. Fortini ME. Notch signaling: the core pathway and its posttranslational regulation. Dev Cell 2009;16:633–47.
27. Micalizzi DS, Christensen KL, Jedlicka P, Coletta RD, Baron AE, Harrell JC, et al. The Six1 homeoprotein induces human mammary carcinoma cells to undergo epithelial-mesenchymal transition and metastasis in mice through increasing TGF-beta signaling. J Clin Invest 2009;119:2678–90.
28. Tang Y, Urs S, Boucher J, Bernaiche T, Venkatesh D, Spicer DB, et al. Notch and transforming growth factor-beta (TGFbeta) signaling pathways cooperatively regulate vascular smooth muscle cell differentiation. J Biol Chem 2010;285:17556–63.
29. Kida Y, Maeda Y, Shiraishi T, Suzuki T, Ogura T. Chick Dach1 interacts with the Smad complex and Sin3a to control AER formation and limb development along the proximodistal axis. Development 2004;131:4179–87.
30. Grego-Bessa J, Diez J, Timmerman L, de la Pompa JL. Notch and epithelial-mesenchyme transition in development and tumor progression: another turn of the screw. Cell Cycle 2004;3:718–21.
31. Weinmaster G, Roberts VJ, Lemke G. A homolog of *Drosophila* Notch expressed during mammalian development. Development 1991;113:199–205.
32. Jadhav AP, Mason HA, Cepko CL. Notch 1 inhibits photoreceptor production in the developing mammalian retina. Development 2006;133:913–23.
33. Artavanis-Tsakonas S, Rand MD, Lake RJ. Notch signaling: cell fate control and signal integration in development. Science 1999;284:770–6.
34. Collins BJ, Kleeberger W, Ball DW. Notch in lung development and lung cancer. Semin Cancer Biol 2004;14:357–64.
35. Konishi J, Kawaguchi KS, Vo H, Haruki N, Gonzalez A, Carbone DP, et al. Gamma-secretase inhibitor prevents Notch3 activation and reduces proliferation in human lung cancers. Cancer Res 2007;67:8051–7.
36. Ji X, Wang Z, Geamanu A, Sarkar FH, Gupta SV. Inhibition of cell growth and induction of apoptosis in non-small cell lung cancer cells by delta-tocotrienol is associated with Notch-1 down-regulation. J Cell Biochem 2011;112:2773–83.
37. Levine M, Hoey T. Homeobox proteins as sequence-specific transcription factors. Cell 1988;55:537–40.
38. Coletta RD, Christensen K, Reichenberger KJ, Lamb J, Micomonaco D, Huang L, et al. The Six1 homeoprotein stimulates tumorigenesis by reactivation of cyclin A1. Proc Natl Acad Sci U S A 2004;101:6478–83.
39. Coletta RD, Christensen KL, Micalizzi DS, Jedlicka P, Varella-Garcia M, Ford HL. Six1 overexpression in mammary cells induces genomic instability and is sufficient for malignant transformation. Cancer Res 2008;68:2204–13.
40. Farabaugh SM, Micalizzi DS, Jedlicka P, Zhao R, Ford HL. Eya2 is required to mediate the pro-metastatic functions of Six1 via the induction of TGF-beta signaling, epithelial-mesenchymal transition, and cancer stem cell properties. Oncogene 2011; Jun 27 [Epub ahead of print].
41. Anami Y, Iijima T, Suzuki K, Yokota J, Minami Y, Kobayashi H, et al. Bronchioloalveolar carcinoma (lepidic growth) component is a more useful prognostic factor than lymph node metastasis. J Thorac Oncol 2009;4:951–8.
42. Colice GL, Rubins J, Unger MAmerican College of Chest P. Follow-up and surveillance of the lung cancer patient following curative-intent therapy. Chest 2003;123:272S–83S.